Algorithms and computations in physics (Oxford Lectures 2025)

Werner Krauth*
Laboratoire de Physique, Ecole normale supérieure, Paris (France)
Rudolf Peierls Centre for Theoretical Physics
University of Oxford (UK)

Fourth lecture: 17 February 2025
(version: 17/02/2025)

This lecture treats classical many-particle systems that interact with a hard-sphere potential. We move from Newtonian mechanics to Boltzmann mechanics and from classical mechanics to statistical mechanics, in a way that, as usual, is entirely example-based. We then treat the case of one-dimensional hard spheres.

Contents

4 Many-particle systems. From Newtonian mechanics to Boltzmann mechanics.

In the hard-sphere model, all configurations have the same potential energy and there is no energetic reason to prefer any configuration over any other. Only entropic effects come into play. In spite of this restriction, hard spheres and disks show a rich phenomenology and exhibit phase transitions from the liquid to the solid state. These "entropic transitions" were once quite unsuspected, and then hotly debated, before they ended up poorly understood, especially in

*werner.krauth@ens.fr, werner.krauth@physics.ox.ac.uk

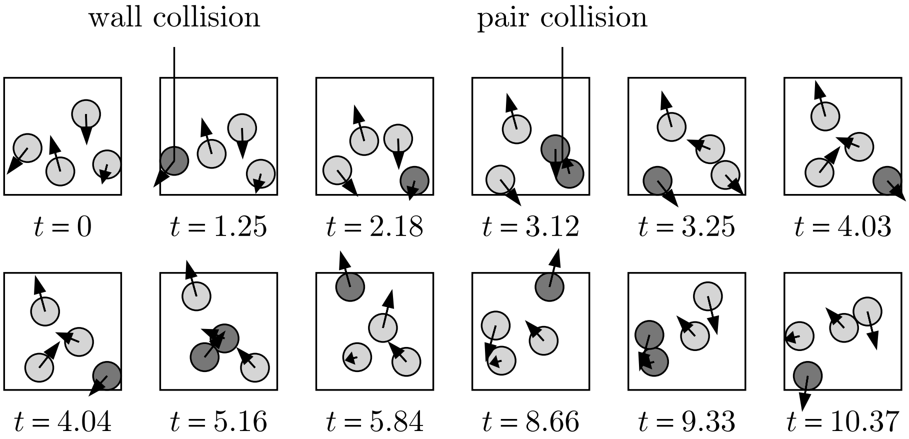

Figure 4.1: Newtonian evolution of four disks in a square box without periodic boundary conditions.

two dimensions. The physics of entropy will occupy us in Lecture 5. In the present lecture, our focus is on the emergence of statistical mechanics from classical mechanics.

4.1 Hard disks—Newton dynamics

We discuss Newtonian dynamics of hard disks, and we will later compare it to the point of view of statistical physics.

4.1.1 Event-driven molecular dynamics

Let us consider a model of hard disks in a box. Disks can undergo collisions with each other or with the walls. To get started with a naive [1] program, we realize that at any generic moment, there are $N(N-1)/2$ pairs of particles which could engage in pair collision, each indexed by a pair-collision time in the future and N individual wall collisions, also in the future. Up to the minimum of these times, the time evolution is straight, and at the next event, either a pair collision or a wall collision takes place (see Alg. 4.1 (`event-disks`)). Look here for a real-life

procedure `event-disks`
input $\{\mathbf{x}_1, \dots, \mathbf{x}_N\}, \{\mathbf{v}_1, \dots, \mathbf{v}_N\}, t$
$\{t_{\text{pair}}, k, l\} \leftarrow$ next pair collision
$\{t_{\text{wall}}, j\} \leftarrow$ next wall collision
$t_{\text{next}} \leftarrow \texttt{min}[t_{\text{wall}}, t_{\text{pair}}]$
for $m = 1, \dots, N$**:**
  $\{\ \mathbf{x}_m \leftarrow \mathbf{x}_m + (t_{\text{next}} - t)\mathbf{v}_m$
if $(t_{\text{wall}} < t_{\text{pair}})$ **then**
  $\{$ **call** `wall-collision` (j)
else:
  $\{$ **call** `pair-collision` (k, l)
output $\{\mathbf{x}_1, \dots, \mathbf{x}_N\}, \{\mathbf{v}_1, \dots, \mathbf{v}_N\}, t_{\text{next}}$
——

Algorithm 4.1: `event-disks`. Event-driven molecular dynamics algorithm for hard disks in a square box of sides 1.

Python program that we will motivate next. We now implement Alg. 4.1 (`event-disks`) without

[1] "naive" means "basically correct, but inefficient".

discretizing time. To do so, we consider an arbitrary pair of particles. They will collide when the norm of their spatial distance vector

$$\underbrace{\mathbf{x}_k(t) - \mathbf{x}_l(t)}_{\Delta\mathbf{x}(t)} = \underbrace{\Delta_{\mathbf{x}}}_{\mathbf{x}_k(t_0)-\mathbf{x}_l(t_0)} + \underbrace{\Delta_{\mathbf{v}}}_{\mathbf{v}_k-\mathbf{v}_l} \cdot (t - t_0) \tag{4.1}$$

equals twice the radius σ of the disks (see Fig. 4.3). This can happen at two times t_1 and t_2, obtained by squaring eq. (4.1), setting $|\Delta\mathbf{x}| = 2\sigma$, and solving the quadratic equation

$$t_{1,2} = t_0 + \frac{-(\Delta_{\mathbf{x}} \cdot \Delta_{\mathbf{v}}) \pm \sqrt{(\Delta_{\mathbf{x}} \cdot \Delta_{\mathbf{v}})^2 - (\Delta_{\mathbf{v}})^2((\Delta_{\mathbf{x}})^2 - 4\sigma^2)}}{(\Delta_{\mathbf{v}})^2}. \tag{4.2}$$

The two disks will collide in the future only if the argument of the square root is positive and if they are approaching each other ($(\Delta_{\mathbf{x}} \cdot \Delta_{\mathbf{v}}) < 0$). The smallest of all the pair collision times obviously gives the next pair collision in the whole system (see Alg. 4.1 (`event-disks`)). Analogously, the parameters for the next wall collision follow from a straightforward time-of-flight analysis.

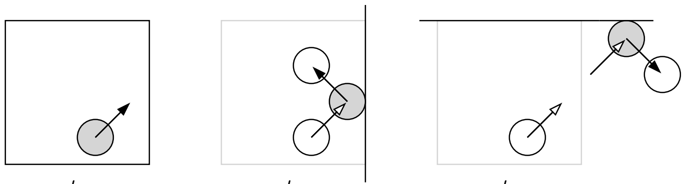

Figure 4.2: Wall collision. The time of a collision is easy to compute, and so is the new velocity

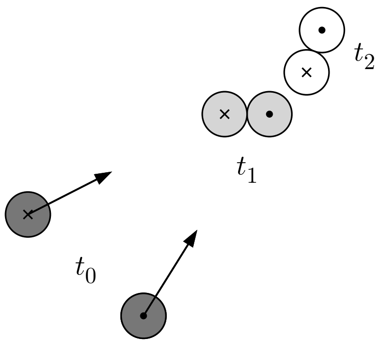

Figure 4.3: Approach of a pair of two disks, as programmed in eq. (4.2)

Pair collisions are best analyzed in the center-of-mass frame of the two disks, where $\mathbf{v}_k + \mathbf{v}_l = 0$ (see Fig. 4.4). Let us write the velocities in terms of the perpendicular and parallel components $\mathbf{v}_\perp$ and $\mathbf{v}_\parallel$ with respect to the tangential line between the two particles when they are exactly in contact. This tangential line can be thought of as a virtual wall from which the particles rebound:

$$\underbrace{\begin{array}{rcl} \mathbf{v}_k & = & \mathbf{v}_\parallel + \mathbf{v}_\perp \\ \mathbf{v}_l & = & -\mathbf{v}_\parallel - \mathbf{v}_\perp \end{array}}_{\text{before collision}}, \quad \underbrace{\begin{array}{rcl} \mathbf{v}'_k & = & \mathbf{v}_\parallel - \mathbf{v}_\perp \\ \mathbf{v}'_l & = & -\mathbf{v}_\parallel + \mathbf{v}_\perp \end{array}}_{\text{after collision}}.$$

The changes in the velocities of particles k and l are $\mp 2\mathbf{v}_\perp$. Introducing the perpendicular unit vector $\hat{\mathbf{e}}_\perp = (\mathbf{x}_k - \mathbf{x}_l)/|\mathbf{x}_k - \mathbf{x}_l|$ allows us to write $\mathbf{v}_\perp = (\mathbf{v}_k \cdot \hat{\mathbf{e}}_\perp)\hat{\mathbf{e}}_\perp$ and $2\mathbf{v}_\perp = (\Delta_{\mathbf{v}} \cdot \hat{\mathbf{e}}_\perp)\hat{\mathbf{e}}_\perp$, where $2\mathbf{v}_\perp = \mathbf{v}'_k - \mathbf{v}_k$ gives the change in the velocity of particle k. The formulas coded into

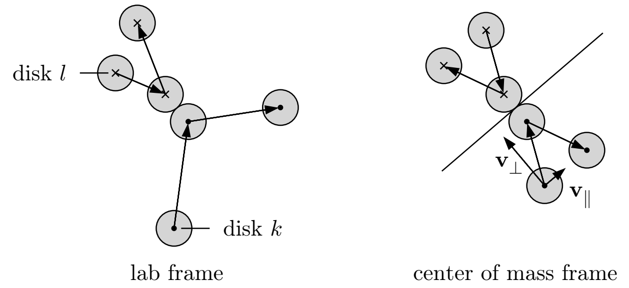

Figure 4.4: Computing the velocities after the pair collision.

procedure `pair-time`
input $\Delta_{\mathbf{x}}$ $(\equiv \mathbf{x}_k(t_0) - \mathbf{x}_l(t_0))$
input $\Delta_{\mathbf{v}}$ $(\equiv \mathbf{v}_k - \mathbf{v}_l \neq 0)$
$\Upsilon \leftarrow (\Delta_{\mathbf{x}} \cdot \Delta_{\mathbf{v}})^2 - |\Delta_{\mathbf{v}}|^2(|\Delta_{\mathbf{x}}|^2 - 4\sigma^2)$
if $(\Upsilon > 0$ and $(\Delta_{\mathbf{x}} \cdot \Delta_{\mathbf{v}}) < 0)$ **then**
$\left\{ t_{\text{pair}} \leftarrow t_0 - \left[(\Delta_{\mathbf{x}} \cdot \Delta_{\mathbf{v}}) + \sqrt{\Upsilon}\right] / \Delta_{\mathbf{v}}^2 \right.$
else:
$\left\{ t_{\text{pair}} \leftarrow \infty \right.$
output t_{pair}
——

Algorithm 4.2: `pair-time`. Pair collision time for two particles starting at time t_0 from positions $\mathbf{x}_k$ and $\mathbf{x}_l$, and with velocities $\mathbf{v}_k$ and $\mathbf{v}_l$.

Alg. 4.3 (`pair-collision`) follow. We note that $\hat{\mathbf{e}}_\perp$ and the changes in velocities $\mathbf{v}'_k - \mathbf{v}_k$ and $\mathbf{v}'_l - \mathbf{v}_l$ are relative vectors and are thus the same in all inertial reference frames. The program can hence be used directly with the lab-frame velocities.

procedure `pair-collision`
input $\{\mathbf{x}_k, \mathbf{x}_l\}$ (particles in contact: $|\mathbf{x}_k - \mathbf{x}_l| = 2\sigma$)
input $\{\mathbf{v}_k, \mathbf{v}_l\}$
$\Delta_{\mathbf{x}} \leftarrow \mathbf{x}_k - \mathbf{x}_l$
$\hat{\mathbf{e}}_\perp \leftarrow \Delta_{\mathbf{x}}/|\Delta_{\mathbf{x}}|$
$\Delta_{\mathbf{v}} \leftarrow \mathbf{v}_k - \mathbf{v}_l$
$\mathbf{v}'_k \leftarrow \mathbf{v}_k - \hat{\mathbf{e}}_\perp(\Delta_{\mathbf{v}} \cdot \hat{\mathbf{e}}_\perp)$
$\mathbf{v}'_l \leftarrow \mathbf{v}_l + \hat{\mathbf{e}}_\perp(\Delta_{\mathbf{v}} \cdot \hat{\mathbf{e}}_\perp)$
output $\{\mathbf{v}'_k, \mathbf{v}'_l\}$
——

Algorithm 4.3: `pair-collision`. Computing the velocities of disks (spheres) k and l after an elastic collision (for equal masses).

4.1.2 Chaos

Algorithm 4.1 (`event-disks`) is entirely deterministic, and we may think that it actually computes the positions and velocities of N hard disks at time t from the values at time $t = 0$. But this is not really the case. It suffices to run the program at different precision levels [2] in order

[2]this is easy to implement in the NumPy extension of Python.

to see that we can really *compute* positions and velocities up to a handful of collisions. Little errors in the numerical computations blow up inexorably, and change the sequence of collisions. This is manifestation of *chaos* that, in our case, is caused by the convex curvature of the disks.

4.1.3 Observables

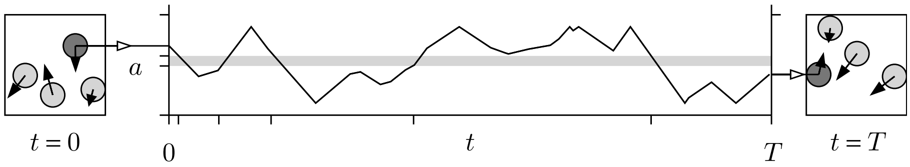

Figure 4.5: Density at position y computed the hard way, by following the entire trajectory

It can be computed exactly for given particle trajectories between times $t = 0$ and $t = T$:

$$\left\{ \begin{array}{c} y\text{-density} \\ \text{at } y = a \end{array} \right\} = \eta_y(a) = \frac{1}{T} \sum_{\substack{\text{intersections } i \\ \text{with gray strip} \\ \text{in Fig. 4.5}}} \frac{1}{|v_y(i)|}. \tag{4.3}$$

In Fig. 4.5, there are five intersections (the other particles must also be considered). At each intersection, $1/|v_y|$ must be added, to take into account the fact that faster particles spend less time in the interval $[a, a + \mathrm{d}a]$, and thus contribute less to the density at a. A more leisurly approach consists in simpy analyzing stroboscopic pictures, that is, intervals. This is the approach we also use for the Monte Carlo algorithm.

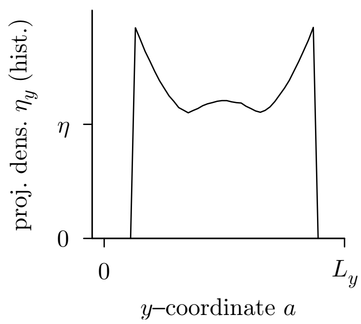

Figure 4.6: Projected density at position y, which is not constant.

4.2 Maxwell distribution, thermostats, Boltzmann distribution

4.2.1 Equal-probability principle for velocities

An obvious differences between molecular dynamics and Monte Carlo consists in that the former has positions and velocities whereas the latter only has positions. We just considered half of the problem, and it is not only the positions that satisfy an equal-probabability condition (under the given constraints) but also the velocities. As we discussed in Lecture 3, positions and velocities are in statistical mechanics distributed independently, both with respect to their Boltzmann distribution

4.3 Hard disks—Boltzmann dynamics

We enter into the discussion of statistical mechanics proper, in the case of the hard-disk model, where things are easier than for general case, that we will sketch in Lecture 5. The basic property that we can study is the equal-probability principle, that means that configurations with the same statistical weight have the same probability.

4.3.1 Equal-probability principle, direct-disk sampling

In the hard-disk case,

$$\pi(\mathbf{x}_1, \ldots, \mathbf{x}_N) = \begin{cases} 1 & \text{if configuration legal} \\ 0 & \text{otherwise} \end{cases}, \tag{4.4}$$

which, as in lecture 1, is to be understood with a Cartesian measure $\mathrm{d}\mathbf{x}_1, \ldots, \mathbf{x}_N$ on both sides. The sampling algorithm consists in the following Algorithm 4.4 (`direct-disks`) is one of a

procedure `direct-disks`
1 **for** $k = 1, \ldots, N$**:**
  $\left\{ \begin{array}{l} x_k \leftarrow \texttt{ran}(x_{\min}, x_{\max}) \\ y_k \leftarrow \texttt{ran}(y_{\min}, y_{\max}) \\ \textbf{for } l = 1, \ldots, k-1\textbf{:} \\ \quad \{ \textbf{ if } \texttt{dist}\,(\mathbf{x}_k, \mathbf{x}_l) < 2\sigma\textbf{:} \quad \textbf{goto } 1 \text{ (reject sample—tabula rasa)} \end{array} \right.$
output $\{\mathbf{x}_1, \ldots, \mathbf{x}_N\}$
——

Algorithm 4.4: `direct-disks`. Direct sampling for N disks of radius σ in a fixed box.

number of direct-sampling algorithms for this system, of which some are even fast, in the limit $N \to \infty$. The *tabula rasa* aspect of it can be understood easily.

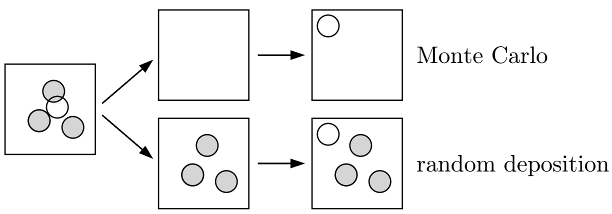

Figure 4.7: Difference between Monte Carlo sampling and the algorithm for random sequential deposition.

4.3.2 Markov-disk sampling (reversible)

We now consider a reversible Markov-chain algorithm for four hard disks in a box.

4.4 Asakura–Oosawa interaction, the fifth force in nature

We discuss the famous Asakura–Oosawa interaction [1], of fundamental importance in biology and soft condensed matter (as for example the physics of polymers).

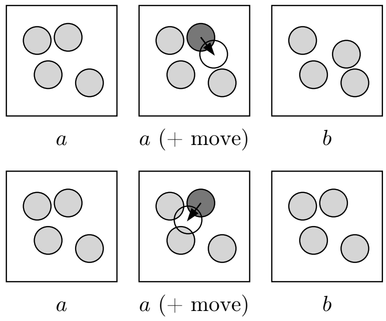

Figure 4.8: Markov-disk algorithm for hard spheres in a box.

procedure `markov-disks`
input $\{\mathbf{x}_1, \ldots, \mathbf{x}_N\}$ (configuration a)
$k \leftarrow \texttt{nran}\,(1, N)$
$\delta\mathbf{x}_k \leftarrow \{\texttt{ran}(-\delta, \delta)\,, \texttt{ran}(-\delta, \delta)\}$
if disk k can move to $\mathbf{x}_k + \delta\mathbf{x}_k$**:** $\mathbf{x}_k \leftarrow \mathbf{x}_k + \delta\mathbf{x}_k$
output $\{\mathbf{x}_1, \ldots, \mathbf{x}_N\}$ (configuration b)
——

Algorithm 4.5: `markov-disks`. Generating a hard-disk configuration b from configuration a using a Markov-chain algorithm (see Fig. 4.8).

4.4.1 The random-clothes-pins model

The random-clothes-pin model [2, Chap. 6] consists in what the name indicates: N clothes-pins (see Fig. 4.9) on a washing line, positioned randomly, as fully defined by Alg. 4.6 (`naive-pin`).

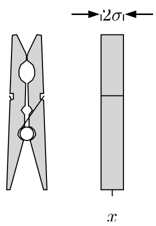

Figure 4.9: A single clothes-pin in side view (*left*) and in front view (*right*). The model is equivalent to one-dimensional hard disks with radius σ.

This model is readily identified as a one-dimensional hard-sphere model with hard-wall boundary conditions. In addition Alg. 4.6 (`naive-pin`) is but a one-dimensional version of the direct-sampling algorithm for hard disks. We can do much better than Alg. 4.6 (`naive-pin`) to sample the positions, namely write the direct-sampling method, implemented in Alg. 4.7 (`direct-pin`). It suffices to realize that on a line of length L with N clothes-pins of diameter 2σ, there is $L - 2N\sigma$ of free space. Miraculously, sampling N random numbers $\texttt{ran}(0, L - 2N\sigma)$, sorting them, then adding back in the 2σ for the clothes-pins is a correct algorithm, although the sort routine, coming out of nowhere, may make us think.

The above algorithms sample the integral:

$$Z_{N,L,=} \int_0^L \mathrm{d}x_1 \;\cdots \int_0^L \mathrm{d}x_N \; \pi(x_1, \ldots, x_N), \tag{4.5}$$

where $\pi = 1$ if the configuration is legal and $\pi = 0$ otherwise. The previous transformation

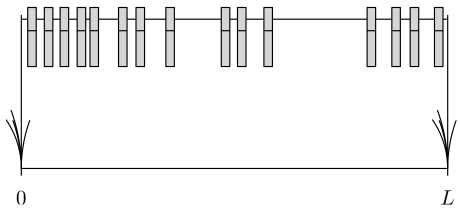

Figure 4.10: $N = 15$ clothes-pins on a washing line of length L.

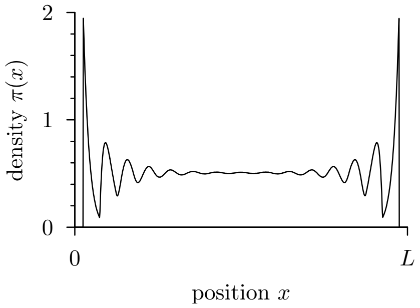

Figure 4.11: Density at position x, obtained by Alg. 4.6 (`naive-pin`)

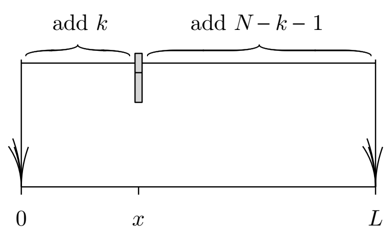

Figure 4.12: Computing the probability of having a clothes-pin at position x.

from the clothes-pins on a line of length L to points on a line of length $L - 2N\sigma$ shows that the partition function must equal:

$$Z_{N,L} = \begin{cases} (L-2N\sigma)^N & \text{if } L > 2N\sigma \\ 0 & \text{otherwise} \end{cases} . \tag{4.6}$$

procedure `naive-pin`
1 **for** $k = 1, \dots, N$:
  $\{$ $x_k \leftarrow \texttt{ran}(\sigma, L-\sigma)$
   for $l = 1, \dots, k-1$:
    $\{$ **if** $|x_k - x_l| < 2\sigma$: **goto** 1 (reject sample—tabula rasa)
output $\{x_1, \dots, x_N\}$
——

Algorithm 4.6: `naive-pin`. Direct-sampling algorithm for N pins of width 2σ on a segment of length L (see Alg. `direct-disks`).

procedure `direct-pin`
for $k = 1, \dots, N$:
  $\{$ $\tilde{y}_k \leftarrow \texttt{ran}(0, L-2N\sigma)$
$\{y_1, \dots, y_N\} \leftarrow \texttt{sort}[\{\tilde{y}_1, \dots, \tilde{y}_N\}]$
for $k = 1, \dots, N$:
  $\{$ $x_k \leftarrow y_k + (2k-1)\sigma$
output $\{x_1, \dots, x_N\}$
——

Algorithm 4.7: `direct-pin`. Rejection-free direct-sampling algorithm for N pins of width 2σ on a line segment of length L.

We may want to check whether the output of Alg. 4.7 (`direct-pin`) is indeed the same as that of Alg. 4.6 (`naive-pin`). Instead, let us obtain the distribution of Fig. 4.11 analytically. Clearly, the probability $\pi(x)$ is given by the total statistical weight of adding k clothes-pins to the left, and $N-k-1$ clothes-pins to the right of the pin at x (see Fig. 4.12), and this gives:

$$\pi(x) = \sum_{k=0}^{N-1} \underbrace{\frac{1}{Z_{N,L}} \binom{N-1}{k} Z_{k,x-\sigma} Z_{N-1-k,L-x-\sigma}}_{\pi_k(x)} . \tag{4.7}$$

where, fortunately, we defined $Z_{N,L}$ even if one cannot fit N clothes-pins into the space L. We may plot eq. (4.7), and convince ourselves that it reproduces Fig. 4.11. The walls thus do attract the clothes-pins. The density there is 4 times larger than in the bulk. It is as if the pins had been glued to the post! Asakura and Oosawa, in a famous paper of 1954 [1], understood that the interaction that we see in Fig. 4.11 is real, and not just a mathematical artifact. To use a drastic statement: replace the clothes-pins by red blood cells, and the two posts by the inner linings of our arteries. The purely entropic attraction of blood cells to the walls (plus some minor details) is what creates heart attacks.

Nevertheless, one might argue that the attraction of the clothes-pins with the walls is but a boundary effect. That this is not true can be seen by placing N pins onto a ring with periodic boundary conditions (see Fig. 4.13). We see that the attraction of the pins to the wall is the same as the mutual attraction of neighboring particles. They also attract each other strongly.

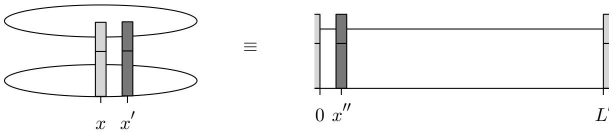

Figure 4.13: Mapping between a pair of clothes-pins on a circle and a single clothes-pin on a washing line.

In conclusion, we have in this section studied the random-clothes-pin model, but have left out one detail, namely Markov-chain Monte Carlo algorithms. This detail has blossomed into its own field [3, 4]. Nevertheless, we have encountered a curious interaction between particles, even if they have no interaction except that of steric hard spheres. We have come up with a curious direct-sampling algorithm which generalizes in some cases to higher dimensions.

4.4.2 Depletion: pictures in one and higher dimensions

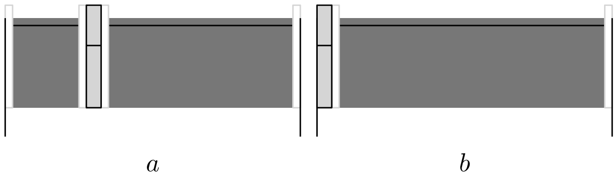

Figure 4.14: Halos at work in the random clothes-pins model for $N = 1$. (a): Halos are attached to the sticks and to the pin, and they do not overlap. (b): Overlapping halos leave more space for the next pin.

The interpretation of the curious interaction between two clothes-pins relies on the concept of a halo. A pin, at position x—the center of the pin—does not allow another pin to lie in the interval $[x - \sigma, x + \sigma]$, because of the wooden material of the pin, but in addition two other intervals $[x - 2\sigma, x - \sigma]$, and $[x + \sigma, x + 2\sigma]$, the *halo*. Halos are attached to the posts, in addition to the pins, but they behave strangely. For example, two halos can overlap, leaving more space for the others (see Fig. 4.14). (which are made of polymers, where depletion is the dominant interaction) polymers. Entropic interactions may also extend beyond soft-condensed-matter physics, as some string theorists have argued [4], with concepts of "emergent gravity" potentially mirroring our emergent "clothes-pin" depletion interaction.

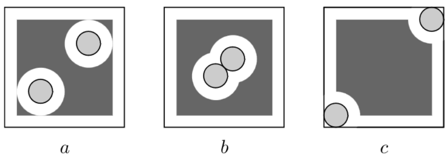

Figure 4.15: Halos in a system of two-dimensional hard disks

4.4.3 Pressure

Unrelated to the above depletion interaction, we wish to discuss the concept of pressure, a fundamental, yet tricky thermodynamic quantity. We may give two representations of the pressure:

1. The (kinetic) pressure is what results, in the system of four hard disks in a square box of length 1, from the bangs of the disks in molecular dynamics at the walls, averaged over time and weighted with a factor $2v^{\perp}$, the velocity normal to the wall.

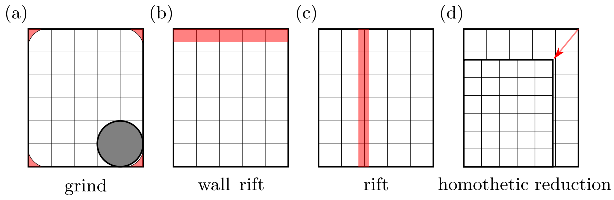

Figure 4.16: Volume changes. Grinding the corners does not reduce the number of configurations with a tiny reduction in volume, but all the other changes can be related to the pressures P_x and P_y.

2. The (thermodynamic) pressure is what results from the fundamental relation: In statistical mechanics, the pressure P is given by the change of the free energy with the system volume:

$$\beta P = \frac{\partial \log Z}{\partial V} = \lim_{V' \to V} \frac{1}{V - V'} \frac{Z - Z'}{Z}, \tag{4.8}$$

with Z the partition function and $Z' \equiv Z(V')$. For hard disks and related models, the rightmost fraction in eq. (5.4) expresses the probability that a sample in the original box of volume V is eliminated in the box of reduced volume $V' < V$ (see Fig. 5.8a-c). In rift-pressure estimators [5], the volume V of an $L_x \times L_y$ box is reduced by removing an infinitesimal vertical or horizontal slab (a "rift"), yielding the components P_x and P_y of the pressure.

The wall rift in Fig. 4.16 is not the most efficient estimator for the pressure but it offers an opportunity to check in one dimension, where we can compute, on the one hand, the pressure using eq. (5.4) and, on the other hand, realize that the configurations that disappear with a wall rift are precisely those with a clothes-pin all the way to the right. Their number is directly related to the density at the wall, and we computed it! EDMD wall-rift estimator:

$$\beta P_x = \frac{1}{2 L_y \tau_{\text{sim}}} \sum_{w:(i, \pm \hat{\mathbf{e}}_x)} \frac{2}{|v^{\perp}_{(i)}|} \tag{4.9a}$$

$$= \left\langle \frac{2}{|v^{\perp}_{\text{wall}}|} \right\rangle \overbrace{\frac{1}{2 L_y \tau_{\text{sim}}} \sum_{w:(i, \pm \hat{\mathbf{e}}_x)} 1}^{\hat{n}^{\pm \hat{\mathbf{e}}_x}_{\text{wall}}} \tag{4.9b}$$

$$= \frac{2\sqrt{\pi}}{\sqrt{\sum v_i^2}} \frac{\Gamma(N + \frac{1}{2})}{\Gamma(N)} \hat{n}^{\pm \hat{\mathbf{e}}_x}_{\text{wall}} \tag{4.9c}$$

$$\xrightarrow{N \to \infty} \sqrt{2\pi\beta m} \hat{n}^{\pm \hat{\mathbf{e}}_x}_{\text{wall}}. \tag{4.9d}$$

Here is the kinematic EDMD estimator

$$P_x = \frac{1}{2 L_y \tau_{\text{sim}}} \sum_{w:(i, \pm \hat{\mathbf{e}}_x)} 2m |v^{\perp}_{\text{wall}}| \tag{4.10a}$$

$$= 2m \left\langle |v^{\perp}_{\text{wall}}| \right\rangle \hat{n}^{\pm \hat{\mathbf{e}}_x}_{\text{wall}} \tag{4.10b}$$

$$= \frac{mR\sqrt{\pi}}{N} \frac{\Gamma(N + \frac{1}{2})}{\Gamma(N)} \hat{n}^{\pm \hat{\mathbf{e}}_x}_{\text{wall}}, \tag{4.10c}$$

$$\xrightarrow{N \to \infty} \sqrt{2\pi\beta m} \hat{n}^{\pm \hat{\mathbf{e}}_x}_{\text{wall}}, \tag{4.10d}$$

The distribution of the velocity perpendicular to a wall is derived from the surface element on the hypersphere of radius $R = \sqrt{v_1^2 + \cdots + v_n^2}$ in $n = 2N$ dimensions:

$$\mathrm{d}\Omega = R^{n-1} \sin^{n-2}\phi_1 \sin^{n-3}\phi_2 \ldots \sin\phi_{n-2} \mathrm{d}\phi_1 \ldots \mathrm{d}\phi_{n-1}, \tag{4.11}$$

where $\phi_1, \ldots, \phi_{n-2} \in [0, \pi]$ and $\phi_{n-1} \in [0, 2\pi]$, and where only $v_1 = R\cos\phi_1$ is expressed in terms of a single angle. It is thus convenient to identify v_1 with $v_{\mathrm{wall}}^{\perp}$. The radius R of the hypersphere at the microcanonical energy $E = mR^2/2$ is related to the inverse temperature in the canonical ensemble as $R^2 = 2N/(m\beta)$. With the integrals

$$\begin{aligned} A &= \int_0^{\pi} \mathrm{d}\phi_1 |\cos\phi_1| \sin^{n-2}\phi_1 = \frac{2}{n-1}, \\ B &= \int_0^{\pi} \mathrm{d}\phi_1 \sin^{n-2}\phi_1 = \sqrt{\pi}\frac{\Gamma[(n-1)/2]}{\Gamma(n/2)}, \end{aligned} \tag{4.12}$$

this yields:

$$\left\langle \frac{1}{|v_{\mathrm{wall}}^{\perp}|} \right\rangle = \frac{1}{R}\frac{B}{A} = \frac{\sqrt{\pi}}{R}\frac{\Gamma(N+\frac{1}{2})}{\Gamma(N)} \xrightarrow{N\to\infty} \sqrt{\frac{\pi m\beta}{2}}, \tag{4.13a}$$

$$\left\langle |v_{\mathrm{wall}}^{\perp}| \right\rangle = R\frac{B}{2NA} = \frac{R\sqrt{\pi}}{2N}\frac{\Gamma(N+\frac{1}{2})}{\Gamma(N)} \xrightarrow{N\to\infty} \sqrt{\frac{\pi}{2m\beta}}, \tag{4.13b}$$

where in the limit $N \to \infty$ the ratio of the Γ functions approaches $\sqrt{N}$. The relative perpendicular velocities $\Delta v_{ij}^{\perp}$ (the projection of the relative velocity $\mathbf{v}_i - \mathbf{v}_j$ perpendicular to the interface separating disks i and j at their collision) is, similarly:

$$\left\langle \frac{1}{|\Delta v_{ij}^{\perp}|} \right\rangle = \frac{\sqrt{2\pi}}{R}\frac{\Gamma(N+\frac{1}{2})}{\Gamma(N)} \xrightarrow{N\to\infty} \sqrt{\pi m\beta}, \tag{4.14a}$$

$$\left\langle |\Delta v_{ij}^{\perp}| \right\rangle = \frac{R\sqrt{\pi}}{\sqrt{2}N}\frac{\Gamma(N+\frac{1}{2})}{\Gamma(N)} \xrightarrow{N\to\infty} \sqrt{\frac{\pi}{m\beta}}. \tag{4.14b}$$

References

[1] S. Asakura and F. Oosawa, "On Interaction between Two Bodies Immersed in a Solution of Macromolecules," *J. Chem. Phys.*, vol. 22, pp. 1255–1256, 1954.

[2] W. Krauth, *Statistical Mechanics: Algorithms and Computations*. Oxford University Press, 2006.

[3] S. C. Kapfer and W. Krauth, "Irreversible Local Markov Chains with Rapid Convergence towards Equilibrium," *Phys. Rev. Lett.*, vol. 119, p. 240603, 2017.

[4] F. H. L. Essler and W. Krauth, "Lifted TASEP: a Bethe ansatz integrable paradigm for non-reversible Markov chains," 2023.